J. Fluid Mech. (2014), *vol.* 752, *pp.* 602–625. © Cambridge University Press 2014
doi:10.1017/jfm.2014.282

Free-stream coherent structures in parallel boundary-layer flows

Kengo Deguchi† and Philip Hall‡

Department of Mathematics, Imperial College London, South Kensington Campus, London SW7 2AZ, UK

(Received 19 December 2013; revised 1 May 2014; accepted 16 May 2014; first published online 9 July 2014)

Our concern in this paper is with high-Reynolds-number nonlinear equilibrium solutions of the Navier–Stokes equations for boundary-layer flows. Here we consider the asymptotic suction boundary layer (ASBL) which we take as a prototype parallel boundary layer. Solutions of the equations of motion are obtained using a homotopy continuation from two known types of solutions for plane Couette flow. At high Reynolds numbers, it is shown that the first type of solution takes the form of a vortex–wave interaction (VWI) state, see Hall & Smith (*J. Fluid Mech.*, vol. 227, 1991, pp. 641–666), and is located in the main part of the boundary layer. On the other hand, here the second type is found to support an equilibrium solution of the unit-Reynolds-number Navier–Stokes equations in a layer located a distance of $O(\ln Re)$ from the wall. Here Re is the Reynolds number based on the free-stream speed and the unperturbed boundary-layer thickness. The streaky field produced by the interaction grows exponentially below the layer and takes its maximum size within the unperturbed boundary layer. The results suggest the possibility of two distinct types of streaky coherent structures existing, possibly simultaneously, in disturbed boundary layers.

Key words: boundary layers, mathematical foundations, nonlinear instability

1. Introduction

In spite of the considerable computer power now available our understanding of the complex physics taking place in transitional or turbulent boundary layers is far from complete. The difficulty in obtaining numerical descriptions of the flows is mostly concerned with the need to resolve structures operating on vastly different length scales. Thus for example in transitional boundary layers the onset of turbulence is associated with rapidly growing secondary instabilities whilst turbulent boundary layers support myriad coherent structures with varying length scales; see Herbert (1988) and Robinson (1991). A number of simplified models have been used in order to analyse the underlying mechanisms of coherent structures observed in both experiments and exhaustive numerical simulations of boundary-layer flows. However, models based on self-consistent asymptotic reductions of the full Navier–Stokes equations are not common. For example, a nonlinear critical-layer theory for pipe flow was developed by Smith & Bodonyi (1982) and its existence at finite Reynolds

† Email address for correspondence: k.deguchi@imperial.ac.uk

‡ Present address: School of Mathematics, Monash University, Melbourne, VIC 3800, Australia.

https://doi.org/10.1017/jfm.2014.282 Published online by Cambridge University Press

number was subsequently confirmed by Deguchi & Walton (2013). Later Smith, Doorly & Rothmayer (1990) extended nonlinear critical-layer theory to suggest possible two-dimensional asymptotic structures in shear flows. These nonlinear critical-layer theories are among the first to indicate subcritical transition in linearly stable flows. However Smith *et al.* (1990) assume the two-dimensionality of the flow and their results are therefore essentially distinct from the structures discussed here.

It is known that turbulent boundary-layer flows involve streaky structures coupled to roll flows in the plane perpendicular to the unperturbed flow; see for example Klein *et al.* (1967) and Kim, Moin & Moser (1987). The streaky flow is unstable to a three-dimensional wave which drives a roll which itself then drives the streak. This three-pointed interaction appeared naturally in the formal asymptotic approach of Hall & Smith (1989, 1990, 1991), and was named vortex–wave interaction theory (VWI) by those authors. The same interaction was also deduced by Waleffe (1997) who analysed numerical data for the type of roll–streak nonlinear equilibrium solutions of shear flows first discovered by Nagata (1990). Following on from the work of Waleffe the interaction was referred to as a self-sustained process.

Direct computations of the Navier–Stokes equations for canonical shear flows such as plane Couette flow or pipe flow have provided a variety of roll–streak-type equilibrium solutions, sometimes called exact coherent structures; see, for example, Faisst & Eckhardt (2003), Waleffe (2003) and Wedin & Kerswell (2004). Calculations motivated by a dynamical systems theory approach have further aided our understanding of such solutions in the turbulence or transition processes; see Gibson, Halcrow & Cvitanovic (2008), Kreilos & Eckhardt (2012), Willis, Cvitanovic & Avila (2013) and many others. The solutions of this type do not bifurcate from the basic flow: instead, the solutions arise as a saddle–node bifurcation as the Reynolds number is increased and develop into what are referred to as lower and upper branch states. Using the Hall & Smith (1991) framework, Hall & Sherwin (2010) more recently showed that the solutions of the asymptotically reduced VWI system can be used to predict the behaviour of full Navier–Stokes solutions with remarkable accuracy even at relatively small Reynolds numbers; see also Blackburn, Hall & Sherwin (2013) where VWI is applied to unbounded shear flows. Subsequently Deguchi & Hall (2014) found that the VWI structure can be embedded in the long-wavelength states found by Deguchi, Hall & Walton (2013). The localized solutions found by Deguchi & Hall (2014) were found to have similarities with turbulent spots.

In the experimental community the distinct properties of coherent structures in the inner and outer regions of boundary-layer flows have long been recognized. Despite the recent success of the asymptotic theories for the roll-streak type of coherent structures located near the wall, several unexplained features remain for the outer-layer coherent structures. These structures are typically characterized by Λ-shape and hairpin-shape vortices rather than rolls and streaks; see Head & Bandyopadhyay (1981), Robinson (1991) and, Adrian, Meinhart & Tomkins (2000). So far the known three-dimensional asymptotic theories do not explain the Reynolds number dependence of the thickness of turbulent boundary layers; but Smith *et al.* (1990) suggest that the two-dimensional structures they propose capture the key scales of turbulent boundary layers.

The relationship between the inner and outer coherent structures has been of much interest in boundary-layer studies. For example, Rao, Narasimha & Narayanan (1971) and Head & Bandyopadhyay (1981) suggested that the vortical structure situated outside of the boundary layer is coupled to the inner boundary-layer structure. In contrast, Jimenez & Pinelli (1999) claimed that the inner and outer coherent structures are independent.

https://doi.org/10.1017/jfm.2014.282 Published online by Cambridge University Press

The aim of the present work is to find the mechanism which supports three-dimensional coherent structures located in the free stream. This is done by finding numerically nonlinear equilibrium solutions and then developing a high-Reynolds-number asymptotic theory which describes them. In this work, we develop a new asymptotic theory motivated by our numerical results for the asymptotic suction boundary-layer flow, which will be referred to as ASBL. This is one of the simplest but yet realizable boundary-layer flows which has constant thickness. Therefore, we do not need to account for the non-parallel effects present in most boundary layers.

The development of the boundary-layer thickness is suppressed by uniform wall suction which is a common laminar flow control technique; for that reason ASBL has attracted much attention. The instability of ASBL was investigated numerically by Hocking (1975) and experimentally by Fransson & Alfredsson (2003). The flow is linearly unstable to Tollmien–Schlichting waves at a Reynolds number $\gtrsim 54\,000$. The nonlinear computation of Milinazzo & Saffman (1985) shows that equilibrium solutions of Tollmien–Schlichting-wave type bifurcate subcritically from the neutral curve and exist at a Reynolds number $\gtrsim 3000$. Direct numerical simulation by Schlatter & Örlü (2011) showed that roll–streak-dominated turbulence with a thick turbulent boundary layer can be sustained at a Reynolds number $\gtrsim 300$. Time-periodic roll–streak-type equilibrium solutions have recently been identified by Khapko *et al.* (2012) and Kreilos *et al.* (2013) by tracing the edge of laminar and turbulent attractors; such edge states for channel flows have also been discussed by Itano & Toh (2001) and Skufca, Yorke & Eckhardt (2006). It is found that the time scale of the roll–streak flow is much longer than that of the wave part of the flow.

In the next section we will write down the governing equations for nonlinear states in ASBL. In § 3 we compute two types of numerical equilibrium solutions in a flow which deforms from plane Couette flow to ASBL. One of the family of equilibrium solutions we find corresponds to VWI states and relates to the results of Khapko *et al.* (2012) and Kreilos *et al.* (2013). In contrast, the other family of equilibrium solutions exhibits new asymptotic states which are completely dependent on the background state being a boundary layer and are found to have an elegant canonical asymptotic form as illustrated in § 4. Finally, in § 5, we give some further discussion and draw some conclusions.

2. Equations of motion

Consider the flow of a viscous fluid of kinematic viscosity ν past the plate defined by $y^* = 0$ with respect to Cartesian coordinates (x^*, y^*, z^*). Suppose that the fluid is sucked from the plate with constant velocity V_0 and that a long way from the plate the x velocity component approaches U_0. In that case the Navier–Stokes equations for the corresponding velocity field $\boldsymbol{u}^* = (u^*, v^*, w^*)$ and pressure p^* must satisfy

$$\boldsymbol{u}^* = (0, -V_0, 0) \quad \text{at } y^* = 0, \tag{2.1}$$

$$\boldsymbol{u}^* \to (U_0, -V_0, 0) \quad \text{as } y^* \to \infty. \tag{2.2}$$

Let us non-dimensionalize the flow using the length scale ν/V_0, time scale $\nu/(U_0 V_0)$, and velocity and pressure scales U_0 and ρU_0^2 respectively where ρ is the fluid density. The Navier–Stokes equations become:

$$(\partial_t + \boldsymbol{u}\cdot\nabla)\boldsymbol{u} = -\nabla p + Re^{-1}\nabla^2\boldsymbol{u}, \tag{2.3}$$

$$\nabla\cdot\boldsymbol{u} = 0. \tag{2.4}$$

https://doi.org/10.1017/jfm.2014.282 Published online by Cambridge University Press

Here the Reynolds number is defined by $Re = U_0/V_0$ and

$$\boldsymbol{\nabla} = (\partial_x, \partial_y, \partial_z), \quad \nabla^2 = \partial^2_{xx} + \partial^2_{yy} + \partial^2_{zz}, \tag{2.5a,b}$$

with x, y, z denoting dimensionless distance in the streamwise, normal and spanwise directions respectively. The appropriate boundary conditions required to completely specify the problem are

$$\boldsymbol{u} = (0, -Re^{-1}, 0) \quad \text{at } y = 0, \tag{2.6}$$
$$\boldsymbol{u} \to (1, -Re^{-1}, 0) \quad \text{as } y \to \infty. \tag{2.7}$$

The solution of the equations of motion corresponding to the unperturbed state is the well-known ASBL profile

$$\boldsymbol{u}_b = (u_b, -Re^{-1}, 0), \tag{2.8}$$

where

$$u_b(y) = 1 - \mathrm{e}^{-y}. \tag{2.9}$$

The basic ASBL given above is an exact solution of the Navier–Stokes equations but the equations of motion and boundary conditions allow for other solutions at sufficiently high Reynolds numbers. The following sections concern these other nonlinear solutions which come into existence with increasing Reynolds number. In the next section we will numerically calculate travelling wave solutions assuming periodicity in the streamwise and spanwise directions and then in § 4 give an asymptotic description of the new type of solutions we find.

3. Nonlinear equilibrium solutions

3.1. *Numerical derivation of the solutions*

We seek nonlinear travelling wave solutions propagating with wave speed c in a box $(x, y, z) \in [0, 2\pi/\alpha] \times [0, H] \times [0, 2\pi/\beta]$. For computational purposes a rigid wall with uniform injection is introduced at a distance H from the lower wall so that the boundary conditions are

$$\boldsymbol{u} = (0, -Re^{-1}, 0) \quad \text{at } y = 0, \tag{3.1}$$
$$\boldsymbol{u} = (1, -Re^{-1}, 0) \quad \text{as } y = H. \tag{3.2}$$

The infinite problem is recovered by taking the limit $H \to \infty$ with all other parameters held fixed. In that case the basic flow is given by (2.8) but with

$$u_b(y) = \frac{1 - \mathrm{e}^{-y}}{1 - \mathrm{e}^{-H}}. \tag{3.3}$$

In the x, z directions we impose periodicity with respective wavenumbers α and β. The spectral code developed in Deguchi *et al.* (2013) to solve channel flow problems is used for this purpose by mapping the wall-normal domain $[0, H]$ to $[-1, 1]$ and adding some extra terms due to the difference of the basic flows. In the numerical code, a Chebyshev basis $T_l(y)$ and Fourier bases $\exp(\mathrm{i}m\alpha(x - ct))$ and $\exp(\mathrm{i}n\beta z)$ are used to discretize the system. The algebraic equations for the spectral coefficients result from a Galerkin projection of the Navier–Stokes equations, and are directly solved by the Newton–Raphson iterative method. The wave speed c is one of the unknowns. The iteration is terminated when the norm of the residual normalized by

https://doi.org/10.1017/jfm.2014.282 Published online by Cambridge University Press

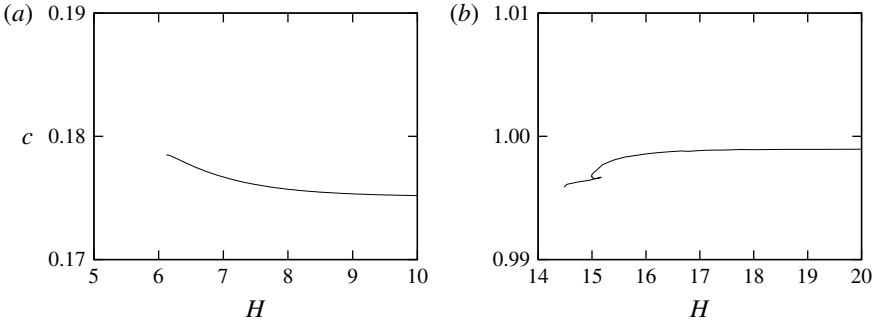


FIGURE 1. The convergence of the wave speed c of with H: (a) the first mode (wall mode) for $(Re, \alpha, \beta) = (80\,000, 0.2, 0.7)$; ($b$) the second mode (FCS) for $(Re, \alpha, \beta) = (80\,000, 0.2, 0.4)$. The truncation levels used in the computations are (a) $(L, M, N) = (140, 5, 50)$ and (b) $(L, M, N) = (140, 7, 18)$.

the norm of the linear part of the equations becomes smaller than 10^{-10}. The spectral expansions are truncated at $l < L$, $|m| < M$, $|n| < N$ with an elliptical cut-off condition. Systematic convergence testing confirms that our solutions are adequately resolved with the truncation level (L, M, N) as specified in the results we give. More detail of the numerical code can be found in Deguchi *et al.* (2013).

In order to find solutions for ASBL, we use a homotopy continuation of solution branches from plane Couette flow. The channel height H plays the role of homotopy parameter since the limit of $H \to 0$, keeping $Re_{PCF} = HRe \sim O(1)$, $\alpha_{PCF} = H\alpha \sim O(1)$ and $\beta_{PCF} = H\beta \sim O(1)$, reduces the ASBL flow to plane Couette flow. Two types of mirror-symmetric plane Couette flow solutions calculated in Deguchi (2013) were used as the starting points of the homotopy. The first one has a single vortex in the normal direction similar to the solution found by Nagata (1990) and corresponds to a travelling wave. The second solution is a stationary equilibrium solution identified in Gibson, Halcrow & Cvitanovic (2009) and Itano & Generalis (2009) with two vortices in the vertical direction. For $H > 0$ both solutions become travelling waves which have the symmetries:

$$[u, v, w](x, y, z) = [u, v, -w](x, y, -z + \pi/\beta), \tag{3.4a}$$

$$[u, v, w](x, y, z) = [u, v, -w](x + \pi/\alpha, y, -z), \tag{3.4b}$$

$$[u, v, w](x, y, z) = [u, v, w](x + \pi/\alpha, y, z + \pi/\beta). \tag{3.4c}$$

In our calculations we began with the two above solutions and increased H until the upper wall plays no role. Figure 1(a,b) illustrates the convergence of our results with increasing H for these solutions. Note that we only present continuation paths for large H, and at lower values of H it was found necessary to also vary Re, α, β when solutions threatened to return to plane Couette flow. The figures show that the second mode has faster wave speed and requires larger values of H to achieve convergence compared to the first mode. We will see in the following subsections that the two ASBL equilibrium solutions have quite distinct high-Reynolds-number asymptotic behaviours.

3.2. *The near-wall coherent structures*

The first kind of solution, hereinafter referred to as the 'wall mode', is related to the VWI structure first outlined in Hall & Smith (1991), and applied to nonlinear

https://doi.org/10.1017/jfm.2014.282 Published online by Cambridge University Press

equilibrium solutions in plane Couette flow by Hall & Sherwin (2010). Here we briefly summarize the asymptotic reduction process of VWI in order to highlight the difference between the two forms of equilibrium solution. Consider equilibrium states propagating with instantaneous wave speed $c(\tau)$ depending on a slow time scale $\tau = Re^{-1}t$. The corresponding VWI state has the asymptotic form

$$\boldsymbol{u} = (U_v, Re^{-1}V_v, Re^{-1}W_v) + Re^{-7/6}[\boldsymbol{u}_w E + \text{c.c.}] + \cdots, \tag{3.5}$$

$$p = Re^{-2}P_v + Re^{-7/6}[p_w E + \text{c.c.}] + \cdots, \tag{3.6}$$

where

$$E = \exp\left[\mathrm{i}\alpha\left(x - Re\int^{\tau} c(\tau')\mathrm{d}\tau'\right)\right], \tag{3.7}$$

and the vortex components $U_v, V_v, W_v, P_v \in \mathbb{R}$ and wave components $u_w, v_w, w_w, p_w \in \mathbb{C}$ are functions of τ, y, z. The streamwise vortex field U_v will be referred to as the streak whilst V_v, W_v constitute the roll flow.

Substituting into the Navier–Stokes equations we find that, away from the critical layer, the equations to determine the roll and streak are

$$(\partial_\tau + \boldsymbol{U}_v \cdot \boldsymbol{\nabla}_{2D})\boldsymbol{U}_v = -\boldsymbol{\nabla}_{2D}P_v + \nabla^2_{2D}\boldsymbol{U}_v, \tag{3.8}$$

$$\boldsymbol{\nabla}_{2D} \cdot \boldsymbol{U}_v = 0, \tag{3.9}$$

where

$$\boldsymbol{\nabla}_{2D} = (0, \partial_y, \partial_z), \quad \nabla^2_{2D} = \partial^2_{yy} + \partial^2_{zz}, \tag{3.10a,b}$$

whilst the wave is determined by solving the generalization of the pressure form of Rayleigh's equation for an inviscid instability of the streak flow:

$$\boldsymbol{\nabla} \cdot \left(\frac{\boldsymbol{\nabla} p_w}{(U_v - c)^2}\right) = 0, \tag{3.11}$$

with vanishing normal derivative conditions at the walls. Equation (3.11) is linear and is a direct consequence of the $Re^{-7/6}$ scaling for the wave; therefore only the leading-order fundamental Fourier mode contributes to the VWI problem.

The equations for the wave are singular at $y = f(\tau, z)$ where $U_v(f(\tau, z), z) = c$. The singularity is smoothed out by viscosity and within the resulting critical layer of thickness $O(Re^{-1/3})$ the Reynolds stresses drive the roll field. The analysis in the critical layer shows that the vortex equations must be solved with the following jumps in roll stress across the critical layer:

$$\left[\partial_n V^s_v(\tau, n, s)\right]^+_- = n_0\alpha^{-5/3}\partial_s\left(\mu^{-5/3}\,|\partial_s p_w|^2\right), \tag{3.12a}$$

$$[P_v]^+_- = -n_0(\alpha\mu)^{-5/3}\Lambda_0\,|\partial_s p_w|^2. \tag{3.12b}$$

Here $V^s_v(\tau, n, s)$ is the roll velocity tangential to the critical layer in the y–z plane, (n, s) are normal and tangential coordinates along the critical layer, Λ_0 is the critical-layer curvature, and $n_0 = 2\pi(2/3)^{2/3}\Gamma(1/3)$. Note that these jump conditions are determined in terms of the wave pressure $p_w(\tau, y, z)$ and the gradient of the streak $\mu = \partial_n U_v$ evaluated on the critical layer. The $Re^{-7/6}$ scaling of the wave has been chosen so that the wave generates $O(1)$ jumps. We note that the VWI mode's critical layer must be situated an $O(1)$ distance from the wall.

https://doi.org/10.1017/jfm.2014.282 Published online by Cambridge University Press

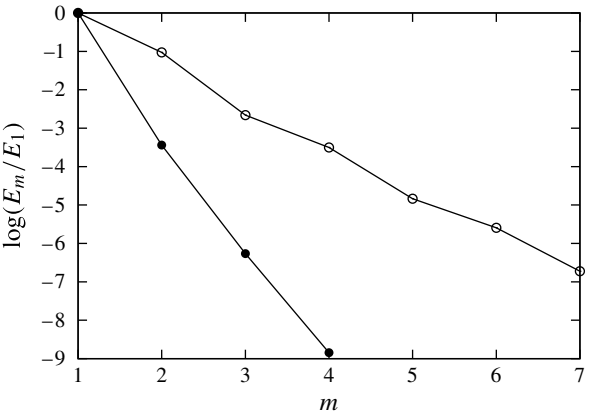


FIGURE 2. The energy density E_m in the mth streamwise Fourier mode for the two types of modes: the closed and open circles correspond to the wall mode and FCS in figure 3, respectively.

Examination of the first type of ASBL solution we find confirms that indeed it is a travelling-wave-type VWI state which is independent of τ. This can be confirmed by increasing the Reynolds number and looking at the scalings of the flow quantities or simply by confirming that the wave energy is concentrated in just the fundamental streamwise Fourier mode: see figure 2 where the energy density for the mth streamwise Fourier mode is shown as filled circles. However we do not give an exhaustive description of the confirmation here since the essential properties of this mode are similar to those found within the plane Couette flow context, see Hall & Sherwin (2010) and Deguchi & Hall (2014).

Figure 3(*a–c*) shows typical flow properties of the wall mode for $(Re, \alpha, \beta, H) = (80\,000,\ 0.2,\ 0.7,\ 10)$. Note that only the deviation of the x-averaged streamwise velocity from the basic solution is pictured in figure 3(*a*) and that subscript 'v' denotes the vortex component of the flow. We see that the flow structure found is entirely consistent with the VWI description: the streaks in figure 3(*a*) and the rolls in figure 3(*b*) are driven by the wave forcing concentrated in a thin critical layer as drawn in figure 3(*c*). The visualizations for this mode are similar to instantaneous snapshots of the periodic mode of Kreilos *et al.* (2013). Note that both of the plane Couette flow solutions we used to begin our calculations were of VWI character.

Within the VWI framework it is clear that τ is the natural time scale over which the roll–streak part of the structure evolves. The full Navier–Stokes edge state calculations of Khapko *et al.* (2012) and Kreilos *et al.* (2013) are apparently finite-Re forms of the VWI states periodic in this slow time scale τ. We predict that the two time scales found numerically in these papers should therefore be in the ratio $1 : Re$ as the Reynolds number varies.

3.3. *The free-stream coherent structures*

Now let us discuss the second type of mode, shown in figure 3(*d–f*). The plots, drawn at $(Re, \alpha, \beta, H) = (80\,000,\ 0.2,\ 0.4,\ 20)$, indicate that the flow structure of this mode clearly differs from the VWI picture. Like the first mode, the streak flow is mainly concentrated near the wall region as shown in figure 3(*d*) but we now see that the roll structure in figure 3(*e*) resides in the free stream. Figure 3(*f*) shows that the forcing

https://doi.org/10.1017/jfm.2014.282 Published online by Cambridge University Press

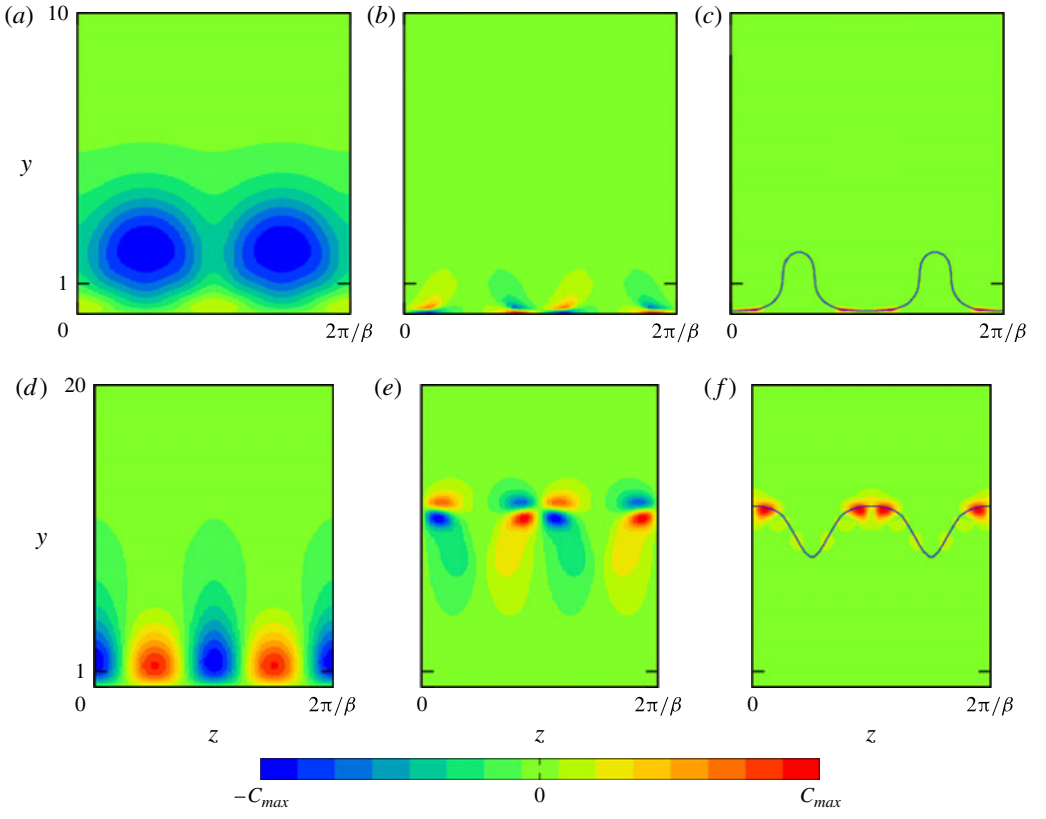


FIGURE 3. (*a,d*) Averaged streamwise velocity distortion $u_v - u_b$. (*b,e*) Averaged streamwise vorticity $(\partial_z v_v - \partial_y w_v)$. Note that (u_v, v_v, w_v) are streamwise-averaged components. (*c,f*) The magnitude of the wave Reynolds stress $F = (F_y^2 + F_z^2)^{1/2}$ where F_y, F_z are the Reynolds stresses acting on the y, z components of the roll. The blue curve is the critical layer $y = f(z)$. (*a–c*) Wall mode, $(Re, \alpha, \beta, H) = (80\,000, 0.2, 0.7, 10)$, the truncation level used in the computation is $(L, M, N) = (130, 4, 45)$; (*d–f*) FCS, $(Re, \alpha, \beta, H) = (80\,000, 0.2, 0.4, 20)$, the truncation level used in the computation is $(L, M, N) = (120, 7, 12)$. The value of C_{max} is (*a*) 7.0×10^{-1}, (*b*) 1.1×10^{-2}, (*c*) 2.9×10^{-6}, (*d*) 2.8×10^{-2}, (*e*) 1.0×10^{-3} and (*f*): 8.6×10^{-8}.

of the roll by the wave is concentrated in the free stream where the wave is found to be concentrated in a layer. The position of the layer is given by the blue curve in figure 3(*f*) where $U_v(f(z), z) = c$, but its depth is thicker than the critical layer we observed in figure 3(*c*), and now comparable to that of the unperturbed boundary layer. The figure suggests that in the layer the roll is generated by the wave Reynolds stresses, and, as in the VWI scenario, is driven by the roll. However, the streak part of the disturbance apparently continues to grow in amplitude moving away from the layer downwards, and takes its maximum in the unperturbed boundary layer before it is reduced to zero as the wall is approached. What is crucial here is that the near-wall streak owes its existence to a nonlinear interaction of much smaller waves taking place out in the free stream.

An examination of this new mode, which we refer to as the 'free-stream coherent structure' (FCS), shows the layer where the waves and rolls are concentrated moves

https://doi.org/10.1017/jfm.2014.282 Published online by Cambridge University Press

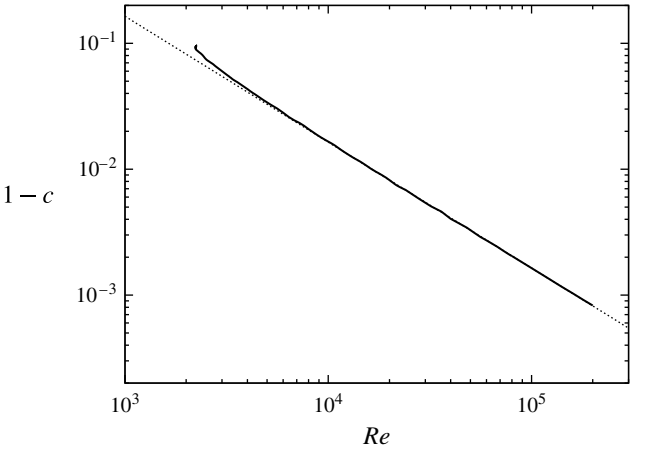


FIGURE 4. Thick solid line is Re dependence of the wave speed for the FCS solutions; $(\alpha, \beta, H) = (0.2, 0.4, 20)$. The truncation level used in the computation is $(L, M, N) = (130, 8, 20)$. The dashed line is $1 - c = c_1/Re$ with $c_1 = 164$.

further away from the lower wall as the Reynolds number increases. As seen in figure 1, the wave propagates downstream with a speed which apparently approaches the free-stream speed. The asymptotic behaviour $1 - c \sim O(Re^{-1})$ is suggested by figure 4. In this figure, the asymptotic line given by analysing high-Reynolds-number numerical results predicts the solution behaviour with remarkable accuracy and thus the FCS solutions seem to be already governed by some asymptotically reduced system with the present values of the Reynolds number. These rather surprising FCS results will be confirmed by the formal asymptotic theory which we shall present in the next section.

A further comparison of the two types of modes is given in figure 5(*a*,*b*). Here rather than plot the deviation, we show the total field including the basic flow. What is important here is that both modes have typical peak–valley streaky fields for the streamwise velocity (shown by the grey surface and colourmap) and the difference between the modes is no longer so apparent. It follows that observations of the streak structure in an experiment or numerical simulation would overlook the crucial difference between the two types of interaction.

A difference between the two modes is observable in the streamwise vorticity contours shown by red and blue surfaces. For the wall mode, the wave field dominates this component and is situated in the near-wall boundary layer; see figure 5(*a*). In contrast the vortices of the FCS are centred in the free stream. The vortices seen in figure 5(*b*) form a Λ shape as observed in the plane Couette flow solution with which the FCS connects. Also the vortices exhibit a slightly shorter structure in the streamwise direction compared to that of figure 5(*a*). This observation is consistent with the energy for the FCS shown in figure 2 where a range of streamwise modes are active for the FCS compared to the wall mode of VWI type. In the next section we give an asymptotic description of the FCS mode and show that indeed, unlike the VWI mode, several streamwise harmonics participate in the interaction.

4. Free-stream coherent structures in the high-Reynolds-number limit

Motivated by the numerical results of the last section we now give a high-Reynolds-number asymptotic description of the FCS. We seek a nonlinear equilibrium state

https://doi.org/10.1017/jfm.2014.282 Published online by Cambridge University Press

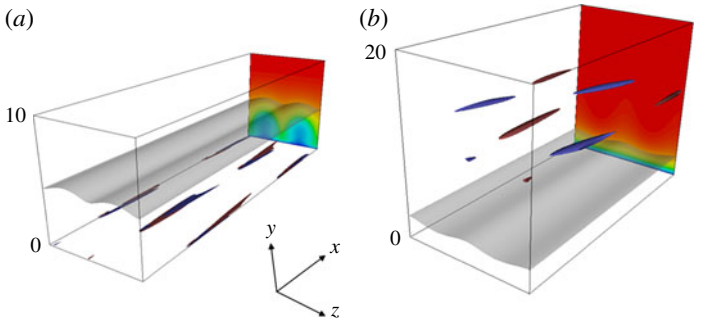


FIGURE 5. Total flow comparison of (*a*) wall mode and (*b*) FCS. The same solutions as figure 3. The colourmap at fixed stream position represents the streamwise velocity at this position (red: free-stream speed, blue: zero). The grey transparent surface is the 80 % maximum of streamwise velocity. The red/blue surfaces are the 80 % maximum/minimum of streamwise vorticity.

concentrated at the edge of the boundary layer, periodic in the streamwise and spanwise directions with wavelengths comparable with the boundary-layer scale so that, based on our original scalings, these are taken to be $O(1)$. Within that layer, which we refer to as the 'production layer', the wave part of the flow, i.e. the part propagating downstream, interacts with the roll and streak in a self-sustaining manner.

A detailed examination of the numerical results suggests that all the disturbance velocity components decay exponentially moving towards the free stream from the production layer, whilst moving downwards from the production layer the roll and streak parts of the disturbance respectively decrease and increase at an exponential rate and the wave part of the flow decays even faster than the roll part. Thus the self-sustaining process which enables the nonlinear state to exist is confined to a layer outside the boundary layer. Our analysis below shows that beneath the production layer there will be an adjustment layer of depth $O(\ln Re)$ and a layer at the wall comparable with the unperturbed boundary-layer thickness. The different asymptotic regions which figure in our analysis are shown in figure 6. An asymptotic layer, located at large distance, of a function involving $\ln Re$ and phase speed approaching free-stream speed was found in the work of Smith *et al.* (1990), Duck, Ruban & Zhikharev (1996) and Dong & Wu (2013). However, the present asymptotic theory, being essentially three-dimensional and nonlinear, has a number of crucial differences to those works as we shall highlight in § 5.

4.1. *The production-layer problem*

The argument we shall now give to derive the interaction equations in the production layer is more closely related to the long-wavelength VWI case discussed by Deguchi *et al.* (2013) for plane Couette flow rather than VWI. The major difference from the long-wavelength interaction is that the streamwise length scale now coincides with the spanwise length scale. The structure we describe is dictated by the fact that the streamwise velocity in the production layer tends to unity plus a small correction comparable to the other two velocity components.

Now consider the streamwise momentum equation where we see that, if viscosity is to play a role in the interaction and the derivatives in all three directions are to remain $O(1)$ so that $\partial^2_{xx} \sim \partial^2_{yy} \sim \partial^2_{zz} \sim O(1)$, then the normal velocity v and spanwise

https://doi.org/10.1017/jfm.2014.282 Published online by Cambridge University Press

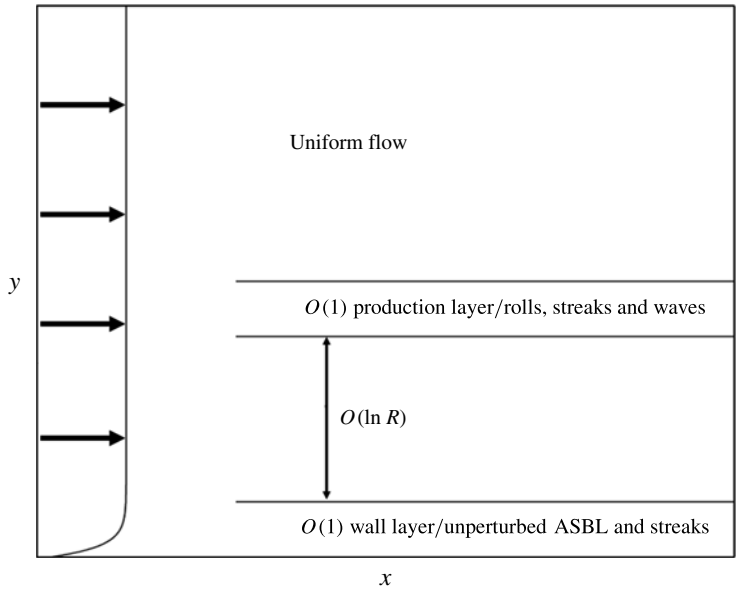


FIGURE 6. The different regions associated with the FCS.

velocity w must be of size $O(Re^{-1})$ to assure the balance of the advection and viscous terms. In that case the term $[\partial_t + u\partial_x]$ in the momentum equations will also be of size $O(Re^{-1})$ given that u differs from free-stream speed by $O(Re^{-1})$. Under this scaling the separation of the equilibrium state into roll, streak and wave cannot be done asymptotically as in VWI theory. Therefore we must allow the wave–roll–streak parts of the flow to be of comparable size and entangled.

Since u includes the basic flow component (3.3) it follows that the production layer is located where $\mathrm{e}^{-y} \sim O(Re^{-1})$. Within this layer the velocity field will satisfy the full Navier–Stokes equations so that nonlinearity can drive the self-sustaining process. The depth of the production layer is fixed as $O(1)$ by insisting that the unperturbed streamwise velocity varies on an $O(1)$ length scale in that layer. Now we define a new variable Y within the production layer as

$$y = \ln Re + Y, \tag{4.1}$$

so that the unperturbed flow in an $O(1)$ layer around $y = \ln Re$ is $1 - Re^{-1}\mathrm{e}^{-Y}$. We assume that the x-dependent part of the flow in the production layer corresponds to a wave moving downstream with almost the speed of the free stream; and since u differs from the free-stream speed by $O(Re^{-1})$, it is reasonable to assume that the wave speed differs from unity by a similar amount. We therefore write

$$X = x - ct, \tag{4.2}$$

$$c = 1 - Re^{-1}c_1 + \cdots . \tag{4.3}$$

The above arguments suggest that in the production layer we seek an asymptotic solution of the Navier–Stokes equations of the form

$$\boldsymbol{u} = (1, 0, 0) + Re^{-1}\boldsymbol{U}(X, Y, z) + \cdots , \quad p = Re^{-2}P(X, Y, z) + \cdots . \tag{4.4a,b}$$

https://doi.org/10.1017/jfm.2014.282 Published online by Cambridge University Press

Note that taking $\boldsymbol{U} = (-\mathrm{e}^{-Y}, -1, 0)$ gives the unperturbed ASBL velocity field and that the time dependence of the wave has been absorbed within X. Note further that we are seeking periodic structures with wavelengths comparable with the boundary-layer thickness, which is constant for ASBL; for more general boundary layers the wavelength will have a different scaling. The production-layer problem is found by substituting the above into the Navier–Stokes equations and retaining leading-order terms to give

$$([\boldsymbol{U} - c_1\boldsymbol{i}]\cdot\boldsymbol{\nabla})\boldsymbol{U} = -\boldsymbol{\nabla}P + \nabla^2\boldsymbol{U}, \tag{4.5}$$

$$\boldsymbol{\nabla}\cdot\boldsymbol{U} = 0. \tag{4.6}$$

At first sight the asymptotic reduction of the problem does not appear significant since we still have the full three-dimensional Navier–Stokes equations. The key point is that they are now to be solved with unit Reynolds number so the reduction is in fact huge.

The numerical solutions given in the previous section suggest that that X-dependence of the flow is confined to the production layer and that above the production layer the flow returns to the uniform flow $(0, -1, 0)$. Below the production layer the results suggest that the velocity at leading order is ASBL flow but with a smaller, exponentially growing disturbance. In addition we impose periodicity in X, z with wavenumbers α, β respectively. Thus the conditions required for the production-layer equations (4.5) and (4.6) in order to determine a nonlinear eigenvalue problem for $c_1 = c_1(\alpha, \beta)$ are

$$\boldsymbol{U}(X, Y, z + 2\pi/\beta) = \boldsymbol{U}(X, Y, z), \tag{4.7}$$

$$\boldsymbol{U}(X + 2\pi/\alpha, Y, z) = \boldsymbol{U}(X, Y, z), \tag{4.8}$$

$$U \to 0, V \to -1, W \to 0 \quad \text{as } Y \to \infty, \tag{4.9}$$

$$U\mathrm{e}^{Y} \to -1, V \to -1, W \to 0 \quad \text{as } Y \to -\infty. \tag{4.10}$$

The production-layer problem we have specified is independent of the Reynolds number and must be solved numerically. Here we will extract the required solution from the results of the previous section. Figure 7 shows the bifurcation diagram of the FCS for a range of values of β against the scaled wave speed $c_1 = Re(1 - c)$. We choose to look at solutions for varying α with the ratio of the wavenumbers held fixed because moving downstream in a growing boundary layer corresponds to the local wavenumbers behaving in that fashion; that will be presented in the future. In the results presented here we have fixed $\alpha/\beta = 0.5$. For the cases corresponding to the solid and dashed lines the channel height is chosen as $H = 20$ and $H = 24$ respectively, whilst the value of Reynolds number is selected as $Re = 200\,000$ so that based on figure 4 the results are safely in the asymptotic range. The crosses correspond to selected points computed with a higher channel height $H = 32$ for $Re = 100\,000$.

It is clear that the solid and dashed curves are converged to the solution of the production-layer problem for $\beta \gtrsim 0.4$ and $\beta \gtrsim 0.3$, respectively. For the converged production-layer results, we see that for a given β there are two solution branches which coalesce at a critical value of $\beta \approx 0.47$; beyond that coalescence no modes were found. Note that the solution presented in § 3 belongs to the upper part of the branch and the lower part of the branch has been found by Newton continuation. Computations for the present range of β show that the velocity fields of production-layer solutions of upper and lower branches are similar and no obvious distinction between them can be seen. For values of β less than those plotted on the two branches

https://doi.org/10.1017/jfm.2014.282 Published online by Cambridge University Press

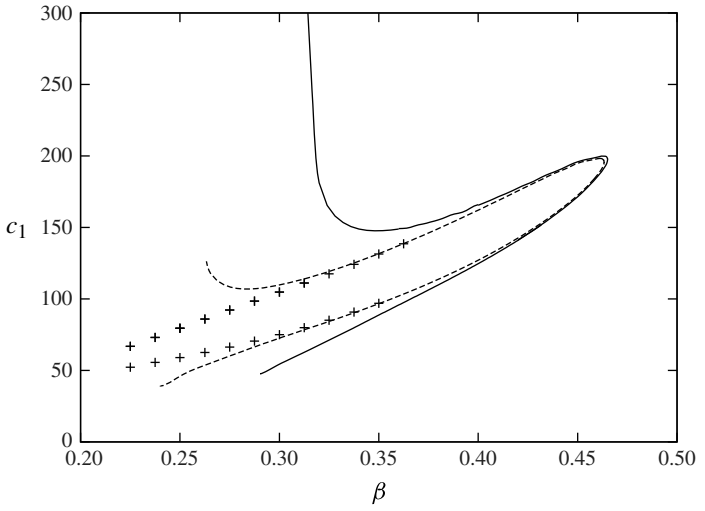


FIGURE 7. The dependence of $c_1 = Re(1 - c)$ for the FCS mode with $\alpha/\beta = 0.5$ and different values of β. The solid curve, dashed curve and crosses correspond to $(Re, H) = (200\,000, 20)$, $(200\,000, 24)$ and $(100\,000, 34)$. The truncation level used in the computation is $(125, 8, 16)$ for $H = 20$, and $(180, 12, 21)$ for $H = 24$ and 34.

we were unable to obtain sufficient resolution to continue the branches so we do not know about the low-β limit of the solutions. The convergence to production-layer states at small β is problematical because in that regime solutions interact with the upper wall and increasingly large values of H must be used in order to find the converged production-layer solutions.

4.2. *The asymptotic behaviour beneath the production layer*

Now let us discuss in more detail the form of the production-layer solutions at $Y = \pm\infty$. In the first instance consider $Y \to \infty$. Here we require that $\boldsymbol{U} \to (0, -1, 0)$ as $Y \to \infty$ so that the flow approaches the uniform flow appropriate to ASBL a long way from the wall. An analysis of (4.5) and (4.6) shows that throughout the production layer, and indeed throughout the flow, the (X, z)-independent part of the normal velocity component is equal to its unperturbed value -1. This means that the streamwise velocity component independent of X, z will at large Y approach zero like e^{-Y}. However, due to nonlinear effects in the production layer, the constant in front of this term will not in general be unity as appropriate to the unperturbed ASBL case. Thus the nonlinear interaction in the production layer can give an $O(1)$ effect on the amplitude of the exponentially decaying streamwise velocity displacement.

Next consider the implications of the conditions (4.10) to be applied as the production layer is exited downwards. Below the production layer the conditions (4.10) require each velocity component to approach their ASBL values at leading order. However, the numerical results of the previous section suggest that the roll part of the disturbance decays exponentially on exiting the production layer whilst the streak part of the disturbance grows exponentially. The decay of the wave is fixed by a balance of diffusion and advection and so it decays faster than the roll which depends only on diffusion.

The origin of the growth of the streak disturbance, which can be decomposed into a mean flow correction and a z-dependent part, is explained by the interaction of the

https://doi.org/10.1017/jfm.2014.282 Published online by Cambridge University Press

decaying roll with the mean part of the basic flow having an exponentially growing form. The interaction of the growing part of the z-dependent part of the streak and roll then leads to a streamwise mean flow correction and this can also grow exponentially but not at the same rate as the z-dependent part of the streak. Whether or not these quantities grow exponentially will be seen below to be a function of the spanwise wavenumber.

In order to analyse the flow beneath the production layer, we decompose the velocity fields into

$$\boldsymbol{U} = (\overline{U}_v(Y), -1, 0) + \boldsymbol{U}_v(Y, z) + \boldsymbol{U}_w(X, Y, z). \tag{4.11}$$

The subscripts v and w denote the vortex and wave parts as in § 3.2 but here we have split the streak component into a mean in z, $\overline{U}_v$, and a z-dependent part U_v. We allow $\overline{U}_v$ to grow exponentially for large negative Y but ultimately it must at leading order reduce to the unperturbed value $-\mathrm{e}^{-Y}$. Note that the vortex field (V_v, W_v) has zero mean in z and that we need not consider the wave part of the flow. The leading-order equations for the vortex components as $Y \to -\infty$ are

$$(\partial^2_{YY} + \partial_Y + \partial^2_{zz})U_v = \mathrm{e}^{-Y}V_v, \tag{4.12}$$

$$(\partial^2_{YY} + \partial_Y + \partial^2_{zz})(\partial^2_{YY} + \partial^2_{zz})\Psi = 0, \tag{4.13}$$

$$\left(\frac{\mathrm{d}^2}{\mathrm{d}Y^2} + \frac{\mathrm{d}}{\mathrm{d}Y}\right)\overline{U}_v = \frac{\beta}{2\pi}\frac{\mathrm{d}}{\mathrm{d}Y}\int_0^{2\pi/\beta}(U_vV_v)\mathrm{d}z, \tag{4.14}$$

where the stream function Ψ associated with the roll flow satisfies $V_v = \partial_z\Psi$, $W_v = -\partial_Y\Psi$. Of great importance in the above equations are the first derivatives with respect to Y: these arise from the '$V\partial_Y$' terms in the production-layer equations with '$V' = -1$. Note that the vortex flow has the mirror-symmetric properties of the solutions (3.4) discussed in the previous section so it has spanwise wavelength half that of the wave part of the flow. Hence if the wavelength of the wave is $(2\pi)/\beta$ then that of the vortex is π/β.

After Fourier analysing in the spanwise directions, we find that for large negative Y the Fourier harmonic of Ψ with wavenumber $2n\beta$ will be given by a combination of two exponentially decaying solutions $\mathrm{e}^{\omega_n Y}$, $\mathrm{e}^{2n\beta Y}$, where

$$\omega_n = \frac{\sqrt{1 + 16n^2\beta^2} - 1}{2} \geqslant 0, \tag{4.15}$$

so that below the production layer the roll normal velocity will behave like

$$V_v \sim \sum_{n=1}^{\infty}(H_n\mathrm{e}^{2n\beta Y} + K_n\mathrm{e}^{\omega_n Y})\cos(2n\beta z), \tag{4.16}$$

where H_n, K_n are constants fixed by the production-layer problem, and from the definition of ω_n we see that for each n the second term decays slowest. The equation for U_v (4.12) forced by this roll solution has the solution

$$U_v \sim \sum_{n=1}^{\infty} J_n\mathrm{e}^{(\omega_n - 1)Y}\cos(2n\beta z) + \cdots. \tag{4.17}$$

https://doi.org/10.1017/jfm.2014.282 Published online by Cambridge University Press

Here the $\cdots$ include decaying exponential terms associated with the unforced equation for U_v and

$$J_n = \frac{K_n}{(\omega_n - 1)^2 + (\omega_n - 1) - 4n^2\beta^2}. \tag{4.18}$$

Noting that $\omega_n - 1 = (\sqrt{1 + 16n^2\beta^2} - 3)/2$ we see that U_v will in fact increase exponentially if

$$\beta < 1/\sqrt{2}. \tag{4.19}$$

For sufficiently small β other higher harmonics of U_v for which $n > 1/\sqrt{2}\beta$ also grow exponentially towards the wall but they will be smaller in magnitude than the fundamental mode.

The roll–streak nonlinear interaction on the right-hand side of (4.14) will be dominated by the exponentially growing U_v mode interacting with the least-decaying V_v mode. It follows that for large negative Y the mean part of the streak $\overline{U}_v$ satisfies

$$\left(\frac{\mathrm{d}^2}{\mathrm{d}Y^2} + \frac{\mathrm{d}}{\mathrm{d}Y}\right)\overline{U}_v \sim \sum_{n=1}^{\infty} \frac{J_n K_n}{2}(2\omega_n - 1)\mathrm{e}^{(2\omega_n - 1)Y} \tag{4.20}$$

so that

$$\overline{U}_v \sim -\mathrm{e}^{-Y} + d_0 + \sum_{n=1}^{\infty} \frac{J_n K_n}{4\omega_n}\mathrm{e}^{(2\omega_n - 1)Y}. \tag{4.21}$$

The first term here is of course the exponential correction to the unperturbed ASBL whilst the third term is forced by the nonlinear interaction within the production layer. The exponential factors within the summation can also lead to exponential growth; however the most rapidly growing one corresponds to $n = 1$ so that we have growth if $\beta < \sqrt{3}/4$.

Thus taking account of the possible growth of the z-dependent part of the streak and writing $Y = y - \ln Re$ we deduce that as the wall layer is approached

$$u \to 1 - \mathrm{e}^{-y} + \frac{d_0}{Re} + \frac{J_1\mathrm{e}^{(\omega_1 - 1)y}}{Re^{\omega_1}}\cos(2\beta z) + \frac{J_1 K_1 \mathrm{e}^{(2\omega_1 - 1)y}}{Re^{2\omega_1} 4\omega_1} + \cdots, \tag{4.22}$$

$$v \to -\frac{1}{Re} + \frac{K_1\mathrm{e}^{\omega_1 y}}{Re^{\omega_1 + 1}}\cos(2\beta z) \tag{4.23}$$

where the $\cdots$ include other growing (but at a smaller rate) harmonics in z. Here $J_1 = K_1/((\omega_1 - 1)^2 + (\omega_1 - 1) - 4\beta^2)$ where K_1 is the constant multiplying the least slowly exponentially decaying part of the roll normal velocity and, together with d_0, is to be determined as part of the production layer solution. Since the wall is reached when $Y = -\ln Re$, we see that the roll is decaying exponentially below the production layer and in fact decays by a factor of $O(Re^{-(\omega_1 + 1)})$ whilst the z-dependent part of the streak becomes $O(Re^{-\omega_1})$ at the wall layer.

Figure 8 shows the dependence of ω_1 on β and we see that whenever $\beta < 1/\sqrt{2}$, there is at least one harmonic of the streak disturbance growing exponentially when $Y \to -\infty$ with the largest growth given by the $n = 1$ mode. In this case we have the rather remarkable result that nonlinear interactions involving velocities of size $O(Re^{-1})$ in the production layer induce a larger change in the streamwise velocity of size $O(Re^{-\omega_1})$ in the main part of the boundary layer. Likewise if $\beta < \sqrt{3}/4$ the mean flow

https://doi.org/10.1017/jfm.2014.282 Published online by Cambridge University Press

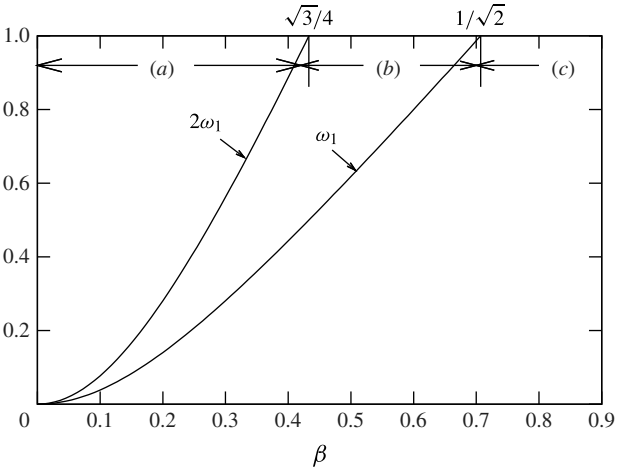


FIGURE 8. The dependence of ω_1 and $2\omega_1$ as functions of β. The labels (a–c) correspond to table 1.

	(a) $\beta < \sqrt{3}/4$	(b) $\sqrt{3}/4 < \beta < 1/\sqrt{2}$	(c) $\beta > 1/\sqrt{2}$
ω_1	$1 > 2\omega_1 > \omega_1$	$2\omega_1 > 1 > \omega_1$	$2\omega_1 > \omega_1 > 1$
$U_v(Y \to -\infty)$	Grow	Grow	Decay
$\overline{U}_v(Y \to -\infty)$	Grow	Constant	Constant

TABLE 1. Summary of the change of solution behaviour beneath the production layer.

correction increases from $O(Re^{-1})$ to be $O(Re^{-2\omega_1})$ in the wall layer. If β is further increased beyond $1/\sqrt{2}$ then the fundamental term can be dropped from the above expansion since the streak disturbance coming out of the production layer decays exponentially. The structure we have given does not fail but the streak disturbance no longer grows beneath the production layer so the effect of the interaction in the production layer is now reduced and simply leads to an $O(Re^{-1})$ correction to the mean flow everywhere beneath the production layer. On the other hand, the induced change in the z-dependent part of the streak varies from $O(Re^{-1})$ to $O(1)$ as β falls from $1/\sqrt{2}$ to zero. Therefore in the long-wavelength limit the change is comparable with the unperturbed flow and the solution fails. These quantitative changes of solution behaviour with varying β are summarized in table 1. The FCS results given in the previous section for $\alpha = 0.2$, $\beta = 0.4$ belong to case (a) in table 1. As seen in figure 7 where the wavenumbers are varied, the solution for case (b) was identified whereas the solution for case (c) is yet to be found.

It remains for us to complete the description of the flow as the unperturbed boundary layer is reached and then near the wall where no-slip conditions must be satisfied. In fact for ASBL we can write down an asymptotic solution in the boundary layer which is valid all the way up to the production layer and matches directly onto the roll–streak flow coming out of the production layer. Since the roll decays below the production layer, the linearized equations (4.12)–(4.14) with Y replaced by y apply all the way to the wall. Therefore in the boundary layer the streamwise and

https://doi.org/10.1017/jfm.2014.282 Published online by Cambridge University Press

normal velocity components are given by

$$u = 1 - \mathrm{e}^{-y} + \frac{\mathrm{d}_0 \overline{u}_2}{Re} + \frac{J_1 u_f}{Re^{\omega_1}} \cos(2\beta z) + \frac{J_1 K_1 \overline{u}_1}{Re^{2\omega_1}} + \cdots, \tag{4.24}$$

$$v = -\frac{1}{Re} + \frac{K_1 v_f}{Re^{\omega_1+1}} \cos(2\beta z) + \cdots. \tag{4.25}$$

Here the functions u_f, v_f are given by

$$u_f(y) = \mathrm{e}^{(\omega_1-1)y} + \frac{B\Omega(\omega_1-1)}{\Omega(-2\beta-1)}\mathrm{e}^{-(2\beta+1)y} - \frac{(B+1)\Omega(\omega_1-1)}{\Omega(-\omega_1-2)}\mathrm{e}^{-(\omega_1+2)y} + G\mathrm{e}^{-(\omega_1+1)y}, \tag{4.26}$$

$$v_f(y) = \mathrm{e}^{\omega_1 y} + B\mathrm{e}^{-2\beta y} - (B+1)\mathrm{e}^{-(\omega_1+1)y}, \tag{4.27}$$

where

$$B = \frac{1+2\omega_1}{2\beta-1-\omega_1}, \quad \Omega(s) = s^2 + s - 4\beta^2, \tag{4.28a,b}$$

and G is chosen so that $u_f(y)$ vanishes at the wall. The functions $\overline{u}_1(y)$ and $\overline{u}_2(y) = 1 - \mathrm{e}^{-y}$ are needed to match the mean flow correction in the wall layer to the exponentially growing mean flow correction beneath the production layer. The function $\overline{u}_1(y)$ is the solution of

$$\left(\frac{\mathrm{d}^2}{\mathrm{d}y^2} + \frac{\mathrm{d}}{\mathrm{d}y}\right)\overline{u}_1 = \frac{1}{2}\frac{\mathrm{d}(u_f v_f)}{\mathrm{d}y} \tag{4.29}$$

and can be expressed in terms of exponential functions but, being rather long and tedious, it is not given here. Our asymptotic description of the FCS for ASBL is now complete. Note that for finite H there exists a layer of $O(1)$ in the vicinity of the upper wall. In this layer we can write down an asymptotic solution of similar exponential form which matches directly to the production-layer solution and satisfies no-slip conditions at the upper wall. Therefore, we can accurately solve the production-layer problem for a finite ASBL problem when the rigid walls are placed at large distance $H \gtrsim \ln Re$ so that the production layer and the upper wall layer do not interact.

4.3. *The asymptotic FCS solution compared to the numerical results*

Here we demonstrate that the full Navier–Stokes calculations in § 3 are in excellent agreement with the asymptotic predictions in the last subsections. In order to confirm the asymptotic structure we decompose the flow field of the numerically obtained equilibrium solutions into

$$\boldsymbol{u}(x-ct, y, z) = (u_b(y) + \overline{u}_v(y), -1, 0) + \boldsymbol{u}_v(y, z) + \boldsymbol{u}_w(x-ct, y, z), \tag{4.30}$$

and define the 'amplitudes'

$$A_{mean}(y) = \sqrt{\langle \overline{u}_v^2 \rangle}, \quad A_{streak}(y) = \sqrt{\langle u_v^2 \rangle}, \tag{4.31a,b}$$

$$A_{roll}(y) = \sqrt{\langle v_v^2 + w_v^2 \rangle}, \quad A_{wave}(y) = \sqrt{\langle u_w^2 + v_w^2 + w_w^2 \rangle}, \tag{4.31c,d}$$

https://doi.org/10.1017/jfm.2014.282 Published online by Cambridge University Press

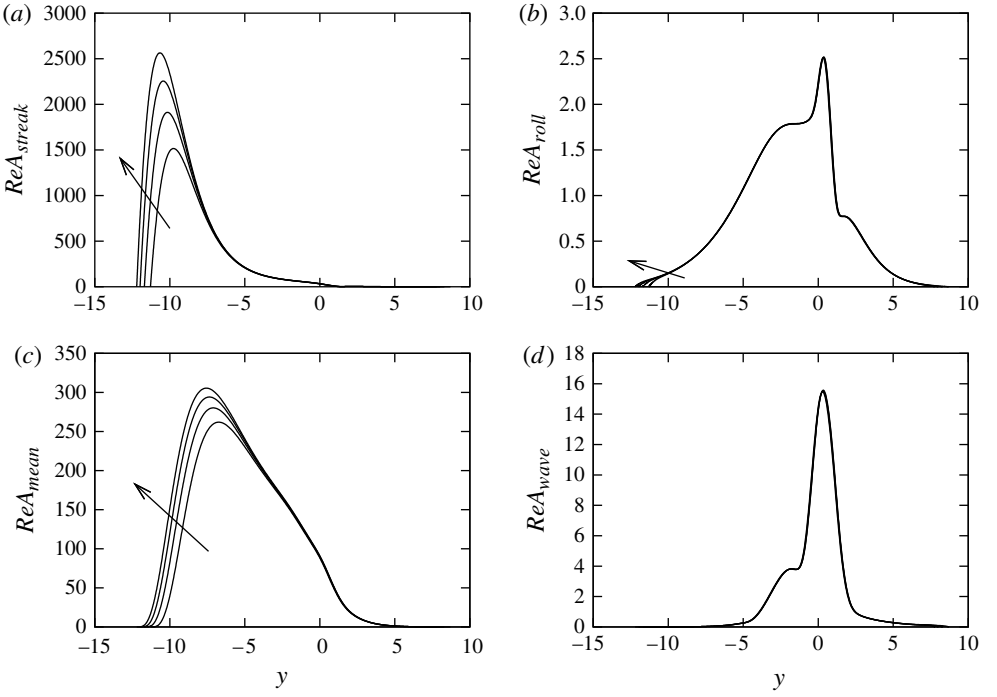


FIGURE 9. Comparison of numerically obtained FCS for various Reynolds numbers in the production layer. The FCS solutions for $Re = 80\,000$, $120\,000$, $160\,000$ and $200\,000$ along the solution branch in figure 4 are used. The curve moves in the direction of the arrows with increasing Re. The definitions of the amplitudes are given in (4.31).

where $\langle * \rangle$ is the x–z average operator defined by

$$\langle * \rangle \equiv \frac{\alpha\beta}{4\pi^2} \int_0^{2\pi/\alpha} \int_0^{2\pi/\beta} * \,\mathrm{d}x\mathrm{d}z. \tag{4.32}$$

For the comparison we select the numerical FCS solutions for $Re = 80\,000$, $120\,000$, $160\,000$ and $200\,000$ with $(\alpha, \beta, H) = (0.2, 0.4, 20)$ which belong to case (a) in table 1. In view of the production-layer scalings (4.4), where each velocity component differed from a uniform flow by $O(Re^{-1})$, we have plotted ReA_{streak}, ReA_{roll}, ReA_{mean}, ReA_{wave} in figure 9. In terms of $Y = y - \ln Re$ the production layer is centred on the origin and here the results for the different Reynolds numbers collapse onto the same curve thereby verifying our production-layer asymptotic description. Consistent with the production-layer theory, the roll and wave are confined to the production layer and the z-dependent part of the streak and the mean flow correction are growing beneath the production layer. Note that for larger negative Y the results do not, as predicted, collapse since distance to the wall changes with Re. We conclude then that the essential part of our high-Re asymptotic structure based on a nonlinear production-layer problem is indeed accurately captured by the FCS solutions found in the final part of the previous section.

This conclusion enables us to extract the value of K_1 from the FCS solutions computed at sufficiently high Re. The value of K_1 fixes the asymptotic form of the

https://doi.org/10.1017/jfm.2014.282 Published online by Cambridge University Press

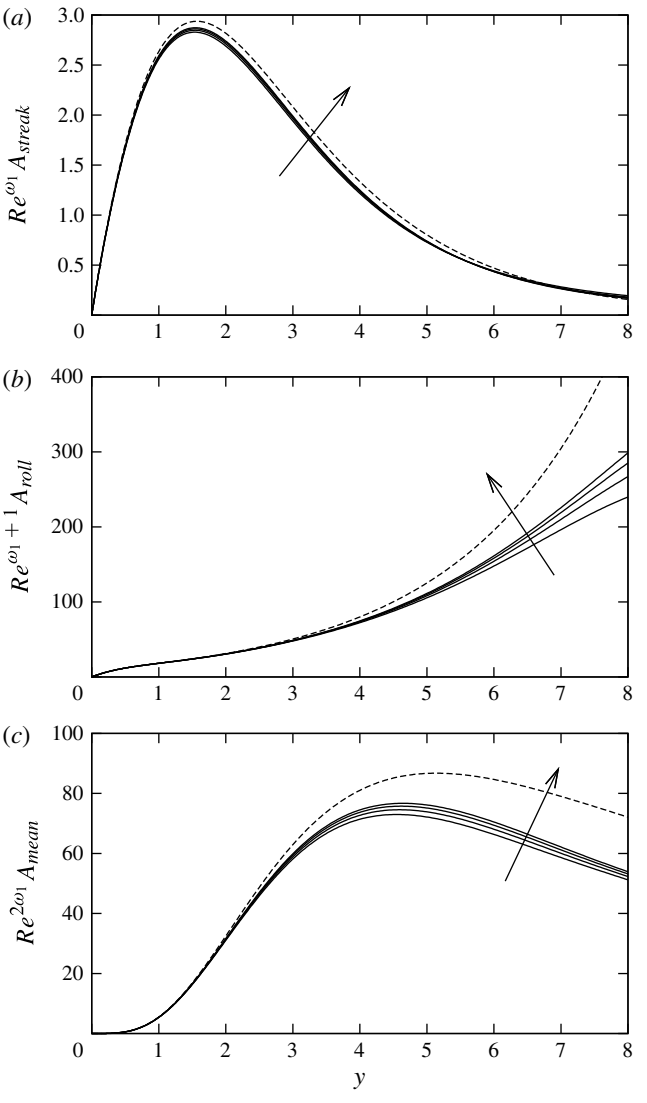


FIGURE 10. Comparison of the numerically obtained FCS for various Reynolds numbers (solid lines) and the corresponding asymptotic solutions ((4.33), dashed lines) in wall layer. The FCS solutions for $Re = 80\,000, 120\,000, 160\,000$ and $200\,000$ along the solution branch in figure 4 are used. The arrows point in the direction of increasing Re. The definitions of the amplitudes are given in (4.31).

amplitude in the wall layer so that

$$A_{streak} = \frac{J_1}{Re^{\omega_1}}\sqrt{\frac{u_f^2}{2}}, \quad A_{roll} = \frac{K_1}{Re^{\omega_1+1}}\sqrt{\frac{v_f^2 + (v_f'/2\beta)^2}{2}}, \quad A_{mean} = \frac{K_1 J_1}{Re^{2\omega_1}}\overline{u}_1. \tag{4.33}$$

The above expressions for case (*a*) in table 1 can be obtained by substituting the leading terms of (4.24) and (4.25) into (4.31). We recall that the wave part decays to zero as confirmed by the wave amplitude plots in figure 9. Figure 10 compares

https://doi.org/10.1017/jfm.2014.282 Published online by Cambridge University Press

the numerical FCS solutions and the asymptotic solution near the wall layer. The choice of the parameter $K_1 = 16.9$ in (4.33) estimated by comparing the numerical and asymptotic amplitude at $y = 1$ gives excellent agreement with the theory and the numerics. With increasing y lower-order terms in (4.24) and (4.25) become important and then the agreement ultimately fails as the production layer is approached and the appropriate structure is given by the production layer forms.

5. Discussion

We have demonstrated that there are at least two types of three-dimensional nonlinear equilibrium solutions in ASBL. The solutions calculated here were found using a homotopy from known plane Couette flow solutions of VWI type. We have shown that for ASBL one type of exact coherent structure is generated near the wall whilst the other type is generated in the free stream though the dominant signature of that mode is a streak near the wall. The high-Reynolds-number asymptotic behaviours of the two types of solution were found to be quite distinct.

The first type of solution, i.e. the wall mode, is closely connected with exact coherent structures in plane Couette flow, and at high Reynolds number it takes on the VWI state of Hall & Sherwin (2010). In VWI the flow in the streamwise direction, i.e. the streak, is driven by a weak roll in the plane perpendicular to that direction. The streak is neutrally stable to an inviscid wave which becomes viscous in a critical layer of $O(Re^{-1/3})$ thickness. Within that layer the wave drives the roll thereby closing the interaction. The VWI character of the interaction is evident in figure 3(*a*) where we observe that the wave forcing is dominated by the contribution in the critical layer where that layer is near the wall. The figure clearly demonstrates the distinctive feature of the wall mode, with the roll generation taking place within the wave critical layer. We also note the large deformation of the boundary layer caused by the streamwise disturbance velocity being of the same size as the unperturbed boundary-layer flow.

The wall mode solution given here has a similar flow structure to the time-periodic solutions recently given by Khapko *et al.* (2012) and Kreilos *et al.* (2013). Their solutions have a travelling-wave-like structure modulated on a long time scale. The dependence of the long time scale on Re was not identified by Khapko *et al.* (2012) and Kreilos *et al.* (2013) but, based on VWI at high Re, we suggest the period is $O(Re)$ times longer than the typical time scale of the wave driving the interaction. Within the VWI formulation the fast time scale is associated with the frequency of the driving wave whilst the slow time scale is associated with the natural relaxation time scale for the roll–streak field.

The nature of the second type of solution we found, the free-stream coherent structure (FCS), is quite different from the wall mode; see figures 3 and 5. The FCS moves downstream with almost the speed of the free stream. Our asymptotic analysis shows that it is generated in a production layer of thickness $O(1)$ located at a distance $O(\ln Re)$ from the wall. In the production layer, each velocity component differs from the basic flow by $O(Re^{-1})$. The asymptotic state of the FCS is determined by the solution of the full Navier–Stokes equations at unit Reynolds numbers subject to periodicity in the streamwise and spanwise directions. The structure is entirely driven by this production-layer problem which we recall is a nonlinear eigenvalue problem for the scaled $O(Re^{-1})$ wave speed. This argument is quite important, since it gives evidence to suggest that free-stream coherent structures are not a passive result of wall streaks but independent self-sustained structures in their own right. Within the

https://doi.org/10.1017/jfm.2014.282 Published online by Cambridge University Press

production layer there is a nonlinear interaction between the roll, streak and wave but these quantities do not separate as in VWI. It should also be pointed out that, as in Deguchi *et al.* (2013), the wave is fully viscous as opposed to the wave of VWI in Hall & Smith (1991) and Hall & Sherwin (2010) which is inviscid over most of the flow.

Moving out of the production layer in either direction the flow returns to the unperturbed boundary layer to leading order, but below the production layer an exponentially growing streak disturbance is generated. The growth rate of the mean (in z) part and z-dependent component of the streak disturbance is controlled by the spanwise wavenumber. For small enough but finite spanwise wavenumbers these components can grow at a slower rate compared to the unperturbed ASBL. However, in the long-spanwise-wavelength limit the z-dependent component grows at the same rate as the unperturbed ASBL and the asymptotic description given breaks down. The streak part of the disturbance grows and reaches a maximum amplitude in the wall layer where it is ultimately reduced to zero.

The characteristic property of the production-layer problem is that nonlinear interactions involving small velocities in this layer can induce a much larger streak disturbance near the wall where no interaction takes place. The mechanism for the generation of the streak disturbance is the interaction of the deviation from unity of the mean part of the streamwise velocity component with the roll in the production layer. As such we might therefore conclude that the FCS structure is special to ASBL because of its strong dependence on the fact that the streamwise basic flow has an exponentially decreasing (as y increases) part directly attributable to the wall suction. However, rather surprisingly, this is not the case and the production-layer structure is considered to be generic to all boundary layers whether parallel or growing, because most boundary layers approach their free-stream value exponentially and boundary-layer growth plays the same role as wall suction. Therefore, the production-layer problem always arises when the advection terms due to this exponential deviation from the free-stream speed and the viscous terms are in balance. For growing boundary layers non-parallel effects mimic the effect of suction so that the same production-layer problem occurs. Although the production-layer problem is still a parallel problem in growing boundary layers, non-parallel effects return beneath the production layer and lead to a totally different downstream development as we shall show in the future.

The FCS and wall mode solutions derived here have spanwise mirror-symmetry and can lead to Λ-shaped vortex structures in the production layer and the main boundary layer respectively. For the FCS in ASBL, the Λ-shaped vortex structure is inherited from the plane Couette flow solution used in our homotopy; see figure 5(*b*). If we associate Λ-shaped vortices with precursors of hairpins this is certainly consistent with experimental observations; see for example Christensen & Adrian (2001). However, here we remark that the widely used visualization techniques such as enstrophy or the so-called 'λ_2' criterion to identify vortex structures confirm that the present FCS solutions lack a 'hairpin head'. If we use the visualization method in Itano & Generalis (2009) then both modes may give hairpin-like structures. However, it is not clear how that visualization can be related to experimental and numerical observations. The production-layer problem is governed by the full Navier–Stokes equations with unit Reynolds number and thus it can potentially have the usually accepted hairpin vortex structure other than the Λ-shaped-vortex-type FCS. A possible candidate for the hairpin vortex solution is a long-wavelength solution continued from our FCS solutions where each pair of the vortex blobs in figure 5(*b*) may be localized in the streamwise direction.

https://doi.org/10.1017/jfm.2014.282 Published online by Cambridge University Press

The role of the FCS from a dynamical systems point of view is of course of interest. For finite values of the spanwise wavenumber β the z-dependent part of the growing FCS streak is at most of size $O(Re^{-\omega_1})$ where $\omega_1 < 1$ is given by (4.15) whilst for the wall mode it is of size $O(1)$. Thus the FCS has smaller amplitude streaks than the wall mode. In other words, the FCS is 'closer' to the unperturbed basic state and thus could be more 'dangerous' in the transition process. It will therefore be interesting to see whether the FCS can play the role of an edge state as Khapko *et al.* (2012) and Kreilos *et al.* (2013) demonstrated was the case for the wall mode. Note that it is possible that in the case investigated by these authors the upper wall was not sufficiently far from the lower one to allow the FCS to exist. It might also be the case that the initial data used in the edge tracking algorithm used by those authors did not have enough structure in the free stream for it to be attracted to the FCS. Note also that the production-layer problem might support further types of solution not found in the present investigation. In particular, the production-layer problem (4.5)–(4.10) can be generalized to the unsteady unit Reynolds number Navier–Stokes equations by replacing c_1 by a slow time derivative. Therefore if periodic solutions of FCS type are identified they do not have the clear separation of scales present in VWI states. The direct numerical simulation of the unsteady production-layer problem to find a more general form of FCS is of particularly interest but yet to be tackled.

An experimental investigation of streak spacing in ASBL induced by free-stream turbulence has been performed by Yoshioka, Fransson & Alfredsson (2004). In an experiment at $Re = 345$ these authors report streak spacing which corresponds to $\beta \approx 0.2$ in our computation where there are two streaks in $z \in [0, 2\pi/\beta]$; see figure 14 of Yoshioka *et al.* (2004). They also reported that the spanwise scale decreases when Re is increased. The streak spacing found experimentally is consistent with the spanwise wavenumbers of the FCS and wall mode solutions computed here. However, we note that in their experiment the measured streak spacing only corresponds to the strongest signal, which is dominated by the wall mode in asymptotic analysis.

Perhaps the most surprising aspect of the FCS is that the maximum streak disturbance is larger than any of the roll, streak and wave fields in the production layer where it is generated. This result suggests a mechanism for small disturbances interacting outside the boundary layer to generate a streak field near the wall. This property could not be found in the two-dimensional asymptotic equilibrium states suggested by Smith *et al.* (1990). Here we further remark that: (i) the FCS is fully viscous whilst in their theory inviscid motion dominates in the nonlinear interaction; (ii) to leading order the FCS does not have the very thin secondary near-wall boundary layer discussed in Smith *et al.* (1990). The impact of free-stream turbulence on Tollmien–Schlichting-wave-type linear instability has been investigated by Duck *et al.* (1996) and Dong & Wu (2013). There it was also found that there is no penetration of free-stream disturbances beyond what is the linearized version of our production layer into the main part of the boundary layer. It is interesting to speculate that free-stream turbulence present in any real flow will resonantly excite the FCS thereby leading to a streak unstable to the waves associated with the wall mode. In that case the role of the FCS in a turbulent boundary layer might be to initiate the streak which then induces a wave travelling within the boundary layer so as to produce the wall mode.

Acknowledgements

The authors wish to acknowledge useful conversations with Professor A. Ruban and Professor X. Wu and the constructive comments made by the referees. We also acknowledge the support of this work by EPSRC through the grant EP/I037946/1.

https://doi.org/10.1017/jfm.2014.282 Published online by Cambridge University Press

REFERENCES

ADRIAN, R. J., MEINHART, C. D. & TOMKINS, C. D. 2000 Vortex organization in the outer region of the turbulent boundary-layer. *J. Fluid Mech.* **422**, 1–54.

BLACKBURN, H. M., HALL, P. & SHERWIN, S. J. 2013 Lower branch equilibria in Couette flow: the emergence of canonical states for arbitrary shear flows. *J. Fluid Mech.* **721**, 58–85.

CHRISTENSEN, K. T. & ADRIAN, R. J. 2001 Statistical evidence of hairpin vortex packets in wall turbulence. *J. Fluid Mech.* **431**, 433–443.

DEGUCHI, K. 2013 Finite amplitude solutions in sliding Couette flow. PhD thesis, Department of Aeronautics, Kyoto University, Japan.

DEGUCHI, K. & HALL, P. 2014 The high-Reynolds-number asymptotic development of nonlinear equilibrium states in plane Couette flow. *J. Fluid Mech.* **750**, 99–112.

DEGUCHI, K., HALL, P. & WALTON, A. G. 2013 The emergence of localized vortex–wave interaction states in plane Couette flow. *J. Fluid Mech.* **721**, 58–85.

DEGUCHI, K. & WALTON, A. G. 2013 A swirling spiral wave solution in pipe flow. *J. Fluid Mech.* **737**, R2.

DONG, M. & WU, X. 2013 On continuous spectra of the Orr–Sommerfeld/Squire equations and entrainment of free-stream vortical disturbances. *J. Fluid Mech.* **732**, 616–659.

DUCK, P. W., RUBAN, A. I. & ZHIKHAREV, C. N. 1996 The generation of Tollmien–Schlichting waves by free-stream turbulence. *J. Fluid Mech.* **312**, 341–371.

FAISST, H. & ECKHARDT, B. 2003 Traveling waves in pipe flow. *Phys. Rev. Lett.* **91**, 224502.

FRANSSON, J. H. M. & ALFREDSSON, P. H. 2003 On the disturbance growth in an asymptotic suction boundary-layer. *J. Fluid Mech.* **482**, 51–90.

GIBSON, J. F., HALCROW, J. & CVITANOVIC, P. 2008 Visualizing the geometry of state space in plane Couette flow. *J. Fluid Mech.* **611**, 107–130.

GIBSON, J. F., HALCROW, J. & CVITANOVIC, P. 2009 Equilibrium and travelling-wave solutions of plane Couette flow. *J. Fluid Mech.* **638**, 243–266.

HALL, P. & SHERWIN, S. 2010 Streamwise vortices in shear flows: harbingers of transition and the skeleton of coherent structures. *J. Fluid Mech.* **661**, 178–205.

HALL, P. & SMITH, F. T. 1989 Nonlinear Tollmien–Schlichting/vortex interaction in boundary-layers. *Eur. J. Mech. (*B*/Fluids)* **8** (3), 179–205.

HALL, P. & SMITH, F. T. 1990 Near planar TS waves and longitudinal vortices in channel flow: nonlinear interaction and focussing. In *Instability and Transition* (ed. M. Y. Hussaini), pp. 5–39. Springer.

HALL, P. & SMITH, F. T. 1991 On strongly nonlinear vortex/wave interactions in boundary-layer transition. *J. Fluid Mech.* **227**, 641–666.

HEAD, M. R. & BANDYOPADHYAY, P. 1981 New aspects of turbulent boundary-layer structure. *J. Fluid Mech.* **107**, 297–337.

HERBERT, T. 1988 Secondary instability of boundary layers. *Annu. Rev. Fluid Mech.* **20**, 487–526.

HOCKING, L. M. 1975 Nonlinear instability of the asymptotic suction velocity profile. *Q. J. Mech. Appl. Maths* **28**, 341–353.

ITANO, T. & GENERALIS, S. C. 2009 Hairpin vortex solution in planar Couette flow: a tapestry of knotted vortices. *Phys. Rev. Lett.* **102**, 114501.

ITANO, T. & TOH, S. 2001 The dynamics of bursting process in wall turbulence. *J. Phys. Soc. Japan* **70**, 703–716.

JIMENEZ, J. & PINELLI, A. 1999 The autonomous cycle of near-wall turbulence. *J. Fluid Mech.* **389**, 335–359.

KHAPKO, T., KREILOS, T., SCHLATTER, P., DUGUET, Y., ECKHARDT, B. & HENNINGSON, D. S. 2012 Localized edge states in the asymptotic suction boundary layer. *J. Fluid Mech.* **717**, R6.

KIM, J., MOIN, P. & MOSER, R. 1987 Turbulence statistics in fully developed channel flow at low Reynolds number. *J. Fluid Mech.* **177**, 133–166.

KLEIN, S. J., REYNOLDS, W. C., SCHRAUB, F. A. & RUNSTADLER, P. W. 1967 The structure of turbulent boundary-layers. *J. Fluid Mech.* **30**, 741–773.

KREILOS, T. & ECKHARDT, B. 2012 Periodic orbits near onset of chaos in plane Couette flow. *Chaos* **22**, 047505.

https://doi.org/10.1017/jfm.2014.282 Published online by Cambridge University Press

KREILOS, T., VEBLE, G., SCHNEIDER, T. M. & ECKHARDT, B. 2013 Edge states for the turbulent transition in the asymptotic suction boundary layer. *J. Fluid Mech.* **726**, 100–122.

MILINAZZO, F. A. & SAFFMAN, P. G. 1985 Finite-amplitude steady waves in plane viscous shear flows. *J. Fluid Mech.* **160**, 281–295.

NAGATA, M. 1990 Three-dimensional finite-amplitude solutions in plane Couette flow: bifurcation from infinity. *J. Fluid Mech.* **217**, 519–527.

RAO, K. N., NARASIMHA, R. & NARAYANAN, M. A. B. 1971 The 'bursting' phenomenon in a turbulent boundary-layer. *J. Fluid Mech.* **48**, 339–352.

ROBINSON, S. K. 1991 Coherent motions in the turbulent boundary-layer. *Annu. Rev. Fluid Mech.* **23**, 601–639.

SCHLATTER, P. & ÖRLÜ, B. 2011 Turbulent asymptotic suction boundary layers studied by simulation. *J. Phys.: Conf. Ser.* **318**, 022020.

SKUFCA, J. D., YORKE, J. A. & ECKHARDT, B. 2006 Edge of chaos in a parallel shear flow. *Phys. Rev. Lett.* **96**, 174101.

SMITH, F. T. & BODONYI, R. J. 1982 Amplitude-dependent neutral modes in the Hagen–Poiseuille flow through a circular pipe. *Proc. R. Soc. Lond.* A **384**, 463–489.

SMITH, F. T., DOORLY, D. J. & ROTHMAYER, A. P. 1990 On displacement-thickness, wall-layer and mid-flow scales in turbulent boundary layers, and slugs of vorticity in channel and pipe flows. *Proc. R. Soc. Lond.* A **428**, 255–281.

WALEFFE, F. 1997 On a self-sustaining process in shear flows. *Phys. Fluids* **9**, 883–900.

WALEFFE, F. 2003 Homotopy of exact coherent structures in plane shear flows. *Phys. Fluids* **15**, 1517–1534.

WEDIN, H. & KERSWELL, R. R. 2004 Exact coherent structures in pipe flow: travelling wave solutions. *J. Fluid Mech.* **508**, 333–371.

WILLIS, A. P., CVITANOVIC, P. & AVILA, M. 2013 Revealing the state space of turbulent pipe flow by symmetry reduction. *J. Fluid Mech.* **721**, 514–540.

YOSHIOKA, S., FRANSSON, J. H. M. & ALFREDSSON, P. H. 2004 Free stream turbulence induced disturbances in boundary layers with wall suction. *Phys. Fluids* **16**, 3530–3539.

https://doi.org/10.1017/jfm.2014.282 Published online by Cambridge University Press